Face-to-Face Contact and Open-Void Coinvolved Si/C Nanohybrids Lithium-Ion Battery Anodes with Extremely Long Cycle Life

Shilong Jing, Hao Jiang, Yanjie Hu, Jianhua Shen, and Chunzhong Li**

To develop high-performance anode materials of lithium-ion batteries (LIBs) instead of commercial graphite for practical applications, herein, a layer of silicon has been well-anchored onto a 3D graphene/carbon nanotube (CNT) aerogels (CAs) framework with face-to-face contact and balanced open void by a simple chemical vapor deposition strategy. The engineered contact interface between CAs and Si creates high-efficiency channels for the rapid electrons and lithium ions transport, and meanwhile, the balanced open-void allows the free expansion of Si during cycling while maintaining high structural integrity due to the robust mechanical strength of 3D CAs framework. As a consequence, the as-synthesized Si/CAs nanohybrids are highly stable anode materials for LIBs with a high reversible discharge capacity (1498 mAh g^{-1} at 200 mA g^{-1}) and excellent rate capability (462 mAh g^{-1} at 10 000 mA g^{-1}), which is much better than Si/graphene-CNTs-mixture (51 mAh g^{-1} at 10 000 mA g^{-1}). More significantly, it is found that the Si/CAs nanohybrids display no obvious capacity decline even after 2000 cycles at a high current density of 10 000 mA g^{-1}. The present Si/CAs nanohybrids are one of the most stable Si-based anode materials ever reported for LIBs to date.

1. Introduction

Rechargeable lithium-ion batteries (LIBs) have been extensively developed to cater to the requirements of various energy applications with higher energy/power densities, e.g., portable electronic devices and electric vehicles.[1,2] The specific capacity of the commercial LIBs has been greatly limited by the widely used graphitic carbon anode materials, which deliver a specific capacity of less than 372 mAh g^{-1} (theoretical value) although they have long cycle life. Starting from the angle of application, it will be a progressive step if we can focus on the modification of carbon materials to further improve the specific capacity without the sacrifice of cycling stability. In this regard, a promising strategy is to hybridize carbon with high capacity active materials. Among them, silicon possesses the highest theoretical capacity (≈3579 mAh g^{-1}, around ten times of graphite), which is reckoned to play a crucial role in boosting the development of next-generation LIBs. Therefore, the Si/C nanohybrids are the most promising anode materials instead of graphite for practical applications.[3–10] However, Si anodes suffer from limited cycle times because of their dramatic volume expansion (>300%) after lithiation as well as poor electrical conductivity.

To get over these limitations, recent significant progresses have been concentrated on the rational construction of Si/C composites for partly improving the capacity at various rates and cycling life by maximizing the synergistic effects among them.[11–17] Thus far, there are two popular strategies to hybridize silicon and carbon. One is to coat a layer of carbon on the surface of silicon nanoparticles (NPs), forming a core/shell nanostructure.[18–24] The specific capacity and rate capability have been remarkably enhanced owing to the full face-to-face contact between silicon and carbon. However, the carbon shell is not expandable enough for maintaining the highly structural integrity, which will undoubtable undergo severe crack and fracture during lithiation/delithiation, resulting in capacity decline rapidly after few tens of cycles. Therefore, another strategy has been developed by incorporating Si NPs into void-containing carbon matrices, forming various yolk-shell nanostructures.[6,13,14,16,25–32] Such void-involved Si/C nanohybrids possess defined internal void space to accommodate the volume change of silicon without destroying the integrity of the electrode materials framework, leading to greatly improved lithium storage performance with prolonged cycle life. Nevertheless, the capacities at various rates are still unsatisfactory considering the contact between silicon and carbon is in point-to-point and/or line-to-line modes, which may be detrimental to the rapid transfer of both electrons and lithium ions due to the frequently ineffective contact caused by the accidental change of the Si/C interface during lithiation/delithiation. Based on the above viewpoints, an ideal Si/C hybrid with high electrochemical performance should have well-contacted Si/C interface and appropriate void space.

Herein, we demonstrate a new insight on the design of a 3D silicon loaded graphene/carbon nanotube (CNT) aerogels (Si/CAs) architecture with ideal Si/C face-to-face contact interface and balanced open void. As shown in **Figure 1**, the CAs

S. Jing, Prof. H. Jiang, Y. Hu, J. Shen, Prof. C. Li
Key Laboratory for Ultrafine Materials of Ministry of Education
School of Materials Science and Engineering
East China University of Science and Technology
Shanghai 200237, P.R. China
E-mail: jianghao@ecust.edu.cn; czli@ecust.edu.cn

DOI: 10.1002/adfm.201502330

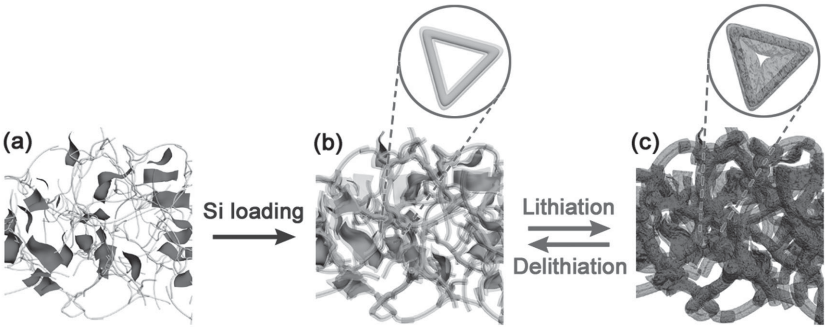

Figure 1. Schematic illustration of the sample structures. a) Graphene/CNTs aerogels (CAs), b) Si/CAs nanohybrids, and c) Li^+-intercalated Si/CAs nanohybrids. The open void of 3D Si/CAs nanohybrids provides the intact face-to-face contact and highly structural integrity in view of the good elasticity and balanced open void of CAs framework during lithiation/delithiation, guaranteeing a long cycle life, as shown in the detailed schematic diagrams.

frameworks are extremely elastic compared with other 3D metal frameworks, e.g., Cu foams, which is favorable for catering to volume change and meanwhile guaranteeing the intact face-to-face contact during lithiation/delithiation even after loading appropriate amounts of silicon. We found that the optimized Si/CAs nanohybrids possess rapid electron/ions transfer and highly structural integrity throughout the whole charge/discharge process. As a consequence, our Si/CAs nanohybrids display a high reversible discharge capacity of 1498 mAh g^{-1} at 200 mA g^{-1} with excellent rate capability (462 mAh g^{-1} at 10 000 mA g^{-1}). More significantly, they show ultralong cycle life, i.e., almost no obvious capacity fading even after over 2000 cycles at 10 000 mA g^{-1}. These excellent electrochemical performances give it huge potential as anode materials for LIBs applications.

2. Results and Discussion

Figure 2a shows the typical scanning electron microscope (SEM) image of the as-synthesized 3D CAs. The graphene and CNTs are well-dispersed and well-interlaced, forming a highly porous architecture. After Si has been uniformly deposited on the CAs framework by a simple CVD method, the resulting Si/CAs nanohybrids are obtained, as shown in Figure 2b,c. Digital photographs of CAs and Si/CAs are also provided in the inset of Figure 2a,b. Here, the CAs will be applied as a rapid electronic transfer network for semiconductive Si. It can be observed that the 3D porous architecture is well-maintained and the Si is also uniformly coated on the surface of CAs framework. The diameter of CNTs coated with Si is about 49 nm. The XRD patterns further confirm the presence of Si, as shown in Figure 2d. The CAs shows a broad peak. After Si deposition, characteristic peaks (2θ) appear at 28°, 47°, and 56°, corresponding to (111), (220), and (311) lattice plane of Si. These results indicate the successful coating of Si layer on CAs.

We perform deep analysis on the microstructure of the Si/CAs nanohybrids by transmission electron microscopy (TEM) and TEM-energy dispersed spectroscopy (EDS) line-scanning and mapping. Figure S1, Supporting Information, shows the TEM image and FTIR curve of CAs, showing that the graphene and CNTs mutually interlaced into a 3D porous structure with rich functional groups. After loading a layer of Si, the absorbing structure is still well-maintained (**Figure 3**a) with much open void space. The elemental distribution across the Si/CNTs is first examined by TEM-EDS line scanning (Figure 3b,c). The profile of Si manifests two peaks on both sides of the C profile, obviously implying the core/shell configuration. A statistical elemental distribution of the Si/CAs nanohybrids is also investigated by TEM-mapping, as shown in Figure S2, Supporting Information. A highly uniform distribution of Si and C can be observed, further demonstrating the Si has been well-deposited on the whole CAs framework. Raman spectroscopy was performed to investigate the crystal form of Si and the structural changes of carbonaceous materials in Si/CAs nanohybrids (Figure 3d). The CAs profile shows two peaks at ≈1340 and ≈1580 cm^{-1}, which are corresponding to the D-band (disordered carbon) and the G-band (graphitic carbon) respectively. After the loading of Si, an intensive peak is demonstrated at ≈490 cm^{-1}, strongly implying the appearance of amorphous Si.[33] Furthermore, due to the consumption of groups on CAs during CVD process,[34] an enhanced I_G/I_D value is observed in Si/CAs nanohybrids,

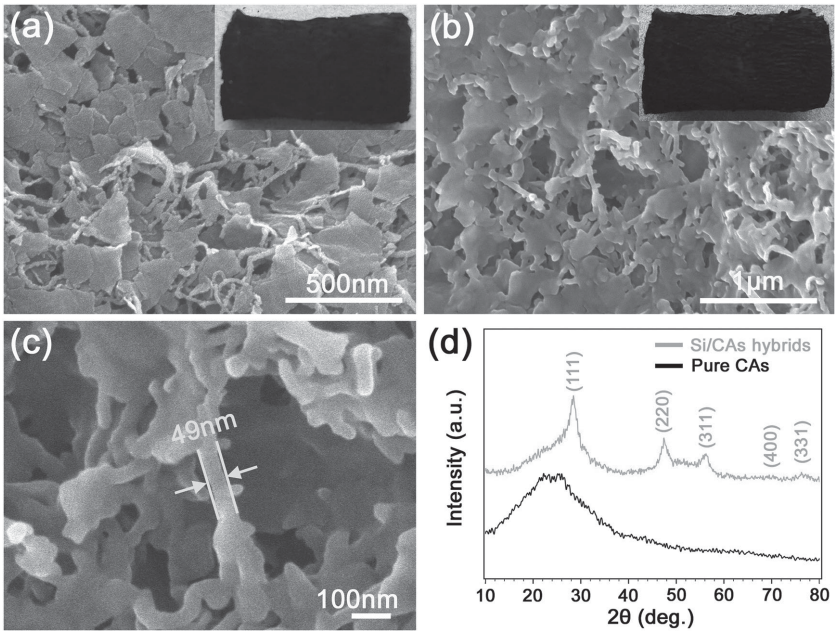

Figure 2. a) SEM image of the CAs, b) low- and c) high-magnification SEM images of the Si/CAs nanohybrids, d) XRD patterns of the Si/CAs nanohybrids and pure CAs. Insets of (a,b) show the digital photographs of CAs and Si/CAs.

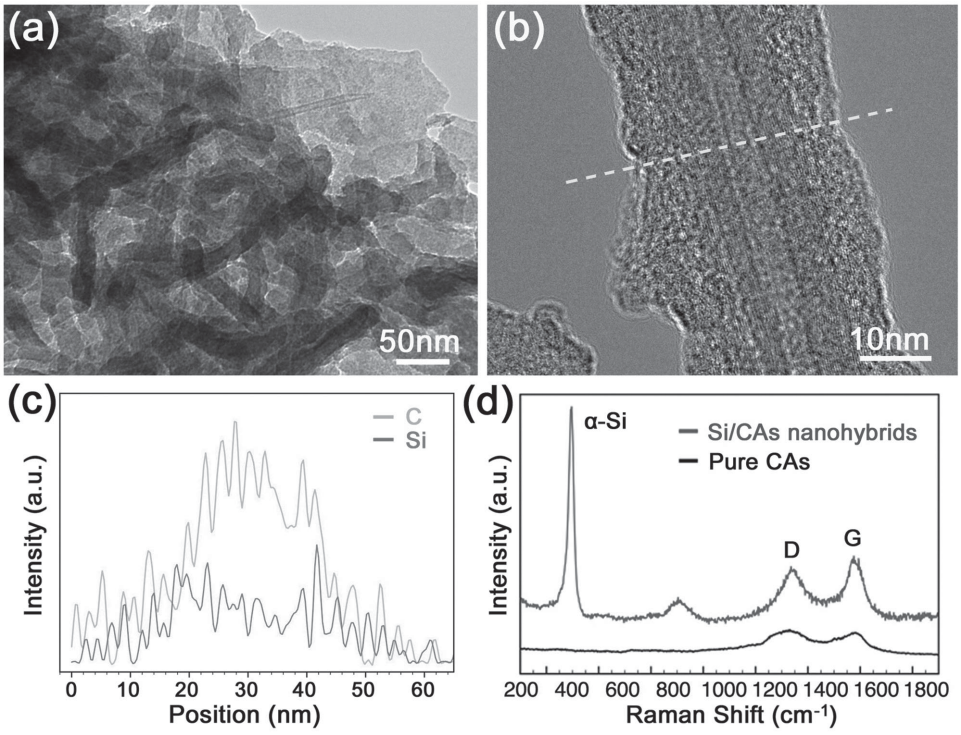

Figure 3. a, b) TEM images, c) line-scanning (indicated by a yellow line in (b) of the Si/CAs nanohybrids, d) Raman spectra of pure CAs (black curve) and Si/CAs nanohybrids (blue curve).

resulting in higher graphitization. Therefore, the amorphous Si layer was deposited on highly graphitized CAs.

The Si content is estimated to be about 50 wt% according to the TGA profile (Figure S3a, Supporting Information). The resulting Si/CAs nanohybrids keep a high specific surface area 74 m^2 g^{-1} with hierarchical pore structures benefitting to the infiltration with electrolyte (Figure S3b, Supporting Information). The Si content can be easily controlled by changing the vapor deposition time, we therefore synthesized the Si/CAs nanohybrids with 25% and 66% Si mass loading, as shown in **Figure 4** and Figure S4, Supporting Information. When the Si content is below 50%, e.g., 25%, the obvious 3D porous structure can be well-maintained. However, for LIBs applications, the low Si content will limit the enhancement of capacity of the Si/C hybrids. After the Si content increased to 66%, a thicker Si has been covered on the CAs framework, resulting in the serious disappearance of the open voids, which will give rise to the structural distortion and crack during charge/discharge process, leading to poor cycle stability. Therefore, an optimal open void for our Si/CAs is very crucial for achieving high power/energy densities and long cycle life.

To obtain the optimal composition, the CAs and the Si/C hybrids with different Si content are then assembled into coin-type half-cells for evaluating their electrochemical performances. The cyclic voltammetry (CV) curves of their first three cycles are shown in **Figure 5**. Upon the first cathodic scans, the CV curves of both pure CAs (Figure 5a) and Si/CAs nanohybrids with 25 wt% Si content (Figure 5b)

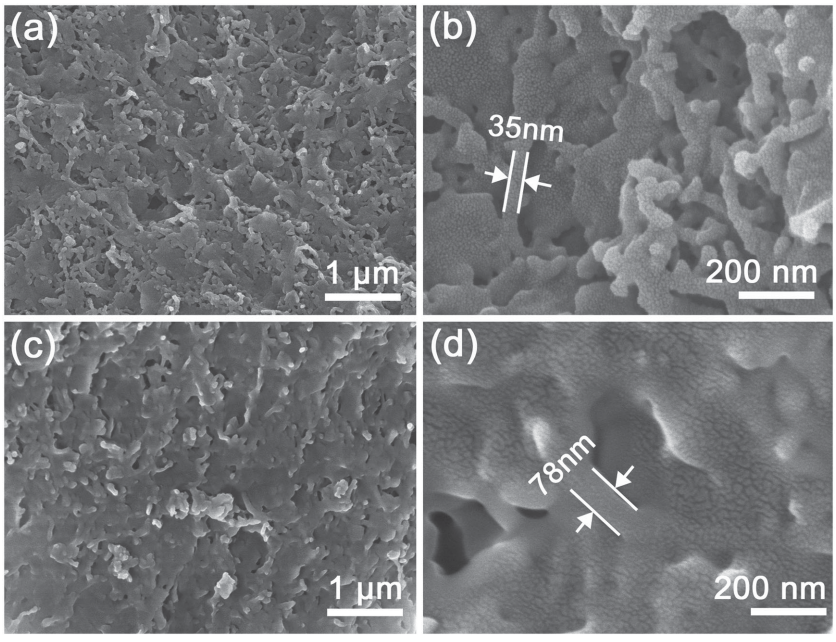

Figure 4. SEM images of the Si/CAs nanohybrids with different mass loading of Si: a,b) 25% and c,d) 66%.

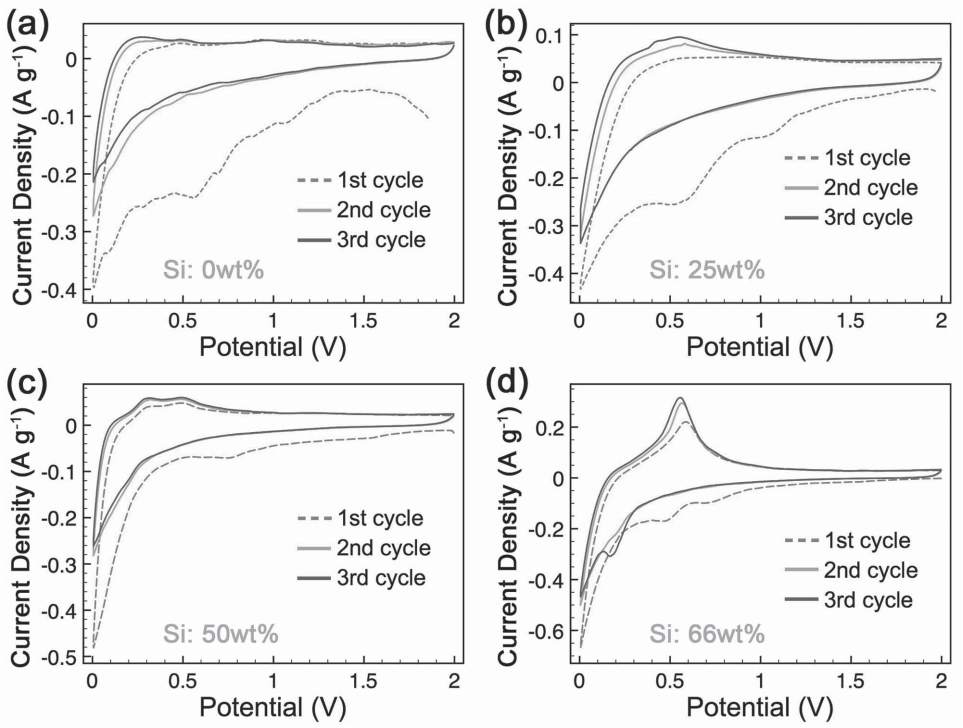

Figure 5. Cyclic voltammetric (CV) curves of the first three cycles for a) pure CAs, b–d) Si/CAs nanohybrids with b) 25 wt%, c) 50 wt%, and d) 66 wt% Si at a scan rate of 0.25 mV s^{-1} between 0.005 and 2.0 V. By integrating the area of CV curves, the Coulombic efficiency of the first cycle from each sample is: a) 17%, b) 27%, c) 33%, and d) 54%.

appear two irreversible peaks at 0.56 and 1.05 V, which are not observed in the other two samples. This is mainly attributed to the presence of partial functional groups on the surface of CAs,[11,16,22] even coating a layer of slight Si. When the mass loading of Si further increases, e.g., 50 wt% (Figure 5c) and 66 wt% (Figure 5d) Si content, more free hydrogen generates from the decomposition of SiH_4, and then reacts with the functional groups of CAs, hence lowering the consumption of irreversible capacity and improving the initial Coulombic efficiency (CE). The capacity retention at various current densities for the Si/CAs nanohybrids with different Si content is then further evaluated by charge/discharge measurements (Figure S5a, Supporting Information). It can be seen that the Si/CAs nanohybrids with 50% Si content possess a comprehensively high electrochemical performance, which is in good agreement with the above CV analysis. To further clarify it, we calculate the respective capacity contribution of CAs and Si in the Si/CAs nanohybrids. The capacity versus Si content plots are shown in Figure S5b, Supporting Information, after fitting the rate performance data. As the fitted lines show, the CAs exhibits steady capacity of ≈600 mAh g^{-1} at different current density. However, the capacity of Si decayed from ≈2200 to ≈380 mAh g^{-1} as the current density increased. Either too little or too much Si content will lead to insufficient overall capacity. Therefore, it is critical to balance the ratio of CAs and Si for comprehensively improving their electrochemical performance. In this work, the Si/C hybrids with 50% Si content are selected for the further investigation on the electrochemical performance.

The initial three charge/discharge curves at 200 mA g^{-1} in the potential window of 0.005–2.0 V are shown in Figure S6, Supporting Information. The first discharge capacity reaches as high as 3168 mAh g^{-1} with an initial CE of 53.7%. In the following two cycles, the discharge capacity can still maintain 1364 and 1263 mAh g^{-1} with a high CE of 93.8% and 99.8%, showing a satisfactory reversibility and stability. We further explored the rate capability of the Si/CAs nanohybrids, as shown in **Figure 6**a. The assembled half-cell is first tested at the same charge/discharge current densities of 200 mA g^{-1}, and then at increased current densities from 400 to 10 000 mA g^{-1}. The Si/CAs nanohybrids deliver a high reversible discharge capacity of 1498, 1128, 841, 726, 588, and 462 mAh g^{-1} at rates of 200, 400, 1000, 2000, 5000, and 10 000 mA g^{-1}, respectively. The galvanostatic discharge/charge profiles of Si/CAs nanohybrids and pure CAs at various current densities have been provided in Figure S7, Supporting Information. It can be seen that the plateau appeared in Si/CAs profiles during the discharge process at various rates, corresponding to the insertion of Li-ion. However, for CAs, the bending slope gradually turned into straight line with the increasing of current density. It turns out that almost of capacity in Si/CAs nanohybrids came from Si (Table S1, Supporting Information). Even at 10 000 mA g^{-1}, about 50% capacity is still contributed by Si. After the deep charge/discharge for five cycles at 10 000 mA g^{-1}, an average capacity of 1088 mAh g^{-1} can be recovered when scanned again at 400 mA g^{-1}, which is about three times of the graphite capacity. To shed light on the importance of aerogels frameworks, we prepared the sample that Si loaded on the freely dispersed graphene and CNTs mixture (denoted as Si/graphene-CNTs-mixture) by the same method. It can be seen that they only show high specific capacity at low current densities for

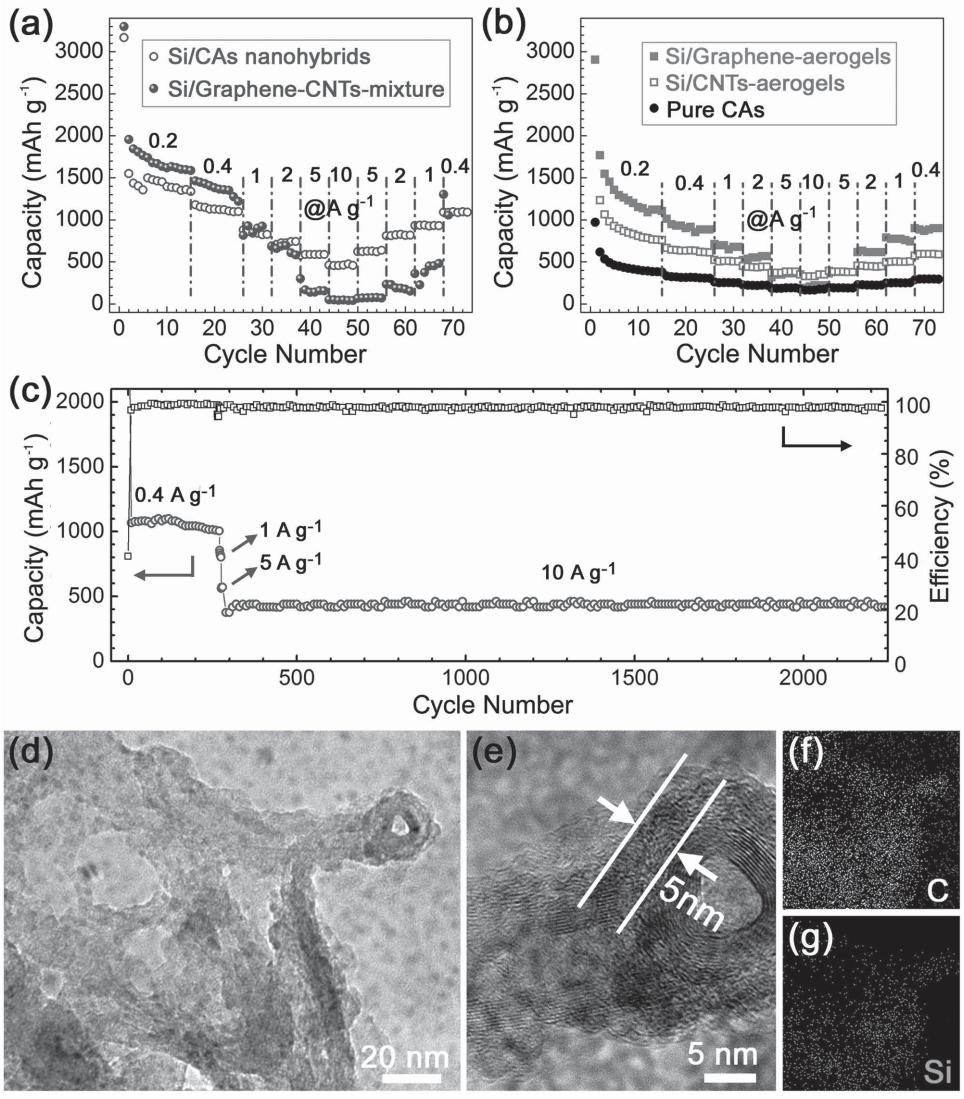

Figure 6. a) The capacity retention of the Si/CAs nanohybrids and Si/graphene-CNTs-mixture at various rates, b) the capacity retention of pure CAs, Si/CNTs-aerogels and Si/graphene-aerogels at various rates, c) cycling performance of the Si/CAs nanohybrids at 400 mA g^{-1} for 270 cycles and subsequent at 10 000 mA g^{-1} for 2000 cycles, d) TEM image, e) high-magnification TEM image, and f,g) the corresponding EDS-mapping of the Si/CAs nanohybrids after 100 cycles.

tens of cycles and subsequent serious capacity fading with the increasing of current densities, as shown in Figure 6a. These results indicate that the leading role of CAs framework in the hybrid as well as the strong synergistic effects between Si and CAs for the remarkable enhancement of electrochemical performance. In addition, we also prepared the pure CAs, Si/CNTs-aerogels and Si/graphene-aerogels using the similar method to better make comparisons. As shown in Figure 6b, our Si/CAs nanohybrids undoubtedly show much higher specific capacity at various rates than pure CAs. Besides, Our Si/CAs nanohybrids also possess much higher specific capacity than Si/CNTs-aerogels and Si/graphene-aerogels at various current densities, further implying higher structural integrity of graphene/CNTs aerogels compared to graphene aerogels and CNTs aerogels.

It is well-known that long cycle life is very important for LIBs practical applications. We first evaluate the cycling stability and the corresponding CE of the Si/CAs nanohybrids at a low current density of 400 mA g^{-1} using a new assembled half-cell, as shown in Figure 6c. It can be seen that the initial reversible capacity is about 1054 mAh g^{-1}, then gradually reaches a maximum value of 1110 mAh g^{-1}, and finally keeps 1015 mAh g^{-1} after 270 cycles. Subsequently, we further evaluate their cycling performance at a very high current density of 10 000 mA g^{-1}. To avoid the damage of batteries, the current gradually increases from 1000 to 5000 mA g^{-1} for five cycles before increasing the current to 10 000 mA g^{-1}. Impressively, no obvious capacity fading can be observed even after another 2000 cycles with almost 100% CE throughout the whole cycles. Such ultralong cycle life with high specific capacity can be mainly ascribed to the elasticity of CAs framework, balanced open-void of the Si/CAs nanohybrids, and full face-to-face contact between them. Detailed speaking, a low Si loading will

result in a relatively large open void space. On this occasion, Si may fall off from the surface of CAs during repeating cycling, and then influencing the subsequent capacity retention. But, a high Si content will reduce void space, leading to serious structural damage due to the remarkable volume change during charge/discharge process. It can be seen that a balanced void space also plays a crucial role in maintaining the structural integrity of the as-obtained Si/CAs nanohybrids. On the other hand, the elasticity of CAs framework is also beneficial for alleviating the structural change. Therefore, the elastic CAs framework with balanced open void in the hybrids guarantees the high structural integrity during cycling. Furthermore, the face-to-face contact of Si and CAs ensure the rich electrochemical active sites and rapid electron transport, leading to a satisfied specific capacity. The electrochemical impedance measurement is also performed to support the above viewpoints. Figure S8, Supporting Information, shows the electrochemical impedance spectra (EIS) of the as-synthesized Si/CAs hybrids before and after cycles. The corresponding charge transfer resistance (R_{ct}) is about 320 and 300 Ω, respectively, almost no sharp changes, further implying a highly structural stability. The full infiltration of electrolyte into the void of Si/CAs hybrids framework may cause the slight decrease of the R_{ct} after cycles.[35] To further understand the superior electrochemical performances of the hybrid structure, a new 2016 coin-type half-cell was assembled, where the binder PVDF was replaced by water-soluble CMC, aiming to bring convenience to the subsequent TEM observation. After 100 cycles, the delithiated anode was rinsed by the distilled water and then characterized by TEM and TEM-EDS mapping. Figure 6d reveals the TEM image of cycled Si/CAs nanohybrids. The 3D framework with many open void is still well-maintained after repeated lithiation/delithiation cycles. As the magnified Si/CNTs shows (Figure 6e), the contact between Si and CAs remains intact without peeling off and crack. Furthermore, a highly uniform distribution of Si and C can be observed from the elemental mapping in Figure 6f,g, directly verifying the highly structural integrity of the Si/CAs nanohybrids.

3. Conclusion

In summary, we demonstrate the synthesis of 3D Si/CAs nanohybrids with full face-to-face contact between Si and CAs as well as well-balanced open void by a simple CVD method, which exhibit excellent and comprehensive electrochemical performances. Detailed speaking, they deliver a high reversible discharge capacity (1498 mAh g^{-1} at 200 mA g^{-1}) and excellent rate capability (462 mAh g^{-1} at 10 000 mA g^{-1}), which is much better than pure CAs (164 mAh g^{-1} at 10 000 mA g^{-1}), Si/graphene-aerogels (205 mAh g^{-1} at 10 000 mA g^{-1}) and Si/CNTs-aerogels (328 at 10 000 mA g^{-1}). Importantly, they also possess a fantastic cycling stability (≈96% capacity retention after 270 cycles at 400 mA g^{-1} and almost no capacity loss after subsequent 2000 cycles at 10 000 mA g^{-1}). Such absorbing electrochemical performances can be mainly attributed to the engineered contact interface between CAs and Si which creates high-efficiency channels for the rapid electrons and lithium ions transport, and meanwhile, the balanced open-void which allows the free expansion of Si during cycling with high structural integrity combining with the robust mechanical strength of 3D aerogels framework. The present Si/CAs nanohybrids show an impressive potential as anode materials for next-generation LIBs.

4. Experimental Section

Synthesis of Graphene/CNTs Aerogels (CAs): For the synthesis of CAs, graphene oxide (GO) and acid treated CNTs with mass ratio of 1:1 were dispersed in distilled water by ultrasonic (power ≈ 150 W, frequency ≈ 20 kHz) for 2 h. After that, resorcinol (R, 2.24 mmol), formaldehyde (F, 4.41 mmol) and Na_2CO_3 (as catalyst, 0.011 mmol) were added to the above solution. The resorcinol-formaldehyde (RF) concentration was estimated to be about 3.58 wt%. The as-obtained solution was cured in petri dish at 85 °C for 72 h. The organic gels were formed, which were further immersed in distilled water for another 48 h for the removal of unreacted RF molecules. The resulting CAs were obtained by the freeze-drying of the clean organic gels and the subsequent pyrolysis process at 1000 °C under inert atmosphere. Similarly, the respective graphene aerogels and CNTs aerogels were also performed using the same method.

Synthesis of Si/CAs Nanohybrids: The above as-synthesized CAs were put into tubular furnace. Silicon deposition was carried out by using SiH_4 gas (5% SiH_4 balance argon) as the precursor at 20 Torr and 650 °C with a flow rate of 250 standard cubic centimeter per minute (sccm) for 20 min. And then, the system was purged with high-purity Ar gas at a flow rate of 500 sccm. When the temperature decreases to below 50 °C, the resulting product was collected. The Si content can be controlled by changing the growth time.

Characterizations: X-ray diffraction (XRD) patterns were collected by using a Rigaku D/max 2550VB/PC X-ray diffractometer with Cu Kα radiation (40 kV, 100 mA). The microstructures of the products were characterized by FESEM (Hitachi S-4800, 5 kV), TEM (JEOL 2010, 200 kV) equipped with an energy dispersive spectrometer (EDS). Nitrogen adsorption–desorption isotherms were measured at 77 K with a Micromeritcs 2010 analyzer. Thermogravimetric analysis (TGA) was measured with a DMA2980/DS analyzer. Raman analysis was measured with an iuvia refl analyzer.

Electrochemical Measurements: The samples (80 wt%), conducting additive (Super-P carbon black, 10 wt%), and polyvinylidene fluoride (PVDF, 10 wt%) binder in *N*-methylpyr-rolidone (NMP) were mixed into homogeneous slurry. The slurry was then pasted onto a copper disk current collector and dried in vacuum at 120 °C. The loading mass and thickness of active materials are about 2.1 mg cm^{-2} and 80 μm. Electrochemical test cells were assembled in an argon-filled glovebox using the coated copper disk as the working electrode, lithium metal foil as the counter/reference electrode, and 1 M solution of $LiPF_6$ in a 1:1 v/v mixture of ethylene carbonate (EC) and dimethyl carbonate (DMC) as the electrolyte. Cyclic voltammetry (CV) of the cells was measured on an Autolab PGSTAT302N electrochemical station. The cells were charged and discharged galvanostatically at different rates in the fixed voltage window from 5 mV to 2 V on a LAND-CT2001A battery tester at room temperature.

Supporting Information

Supporting Information is available from the Wiley Online Library or from the author.

Acknowledgements

This work was supported by the National Natural Science Foundation of China (21206043, 21236003), the Shanghai Shuguang Scholars Program (13SG31), the Shanghai Rising-Star Program (13QA1401100,

15QA1401200), the 111 Project (B14018), and the Fundamental Research Funds for the Central Universities.

Received: June 8, 2015
Revised: June 29, 2015
Published online: July 27, 2015

[1] M. Armand, J.-M. Tarascon, *Nature* **2008**, *451*, 652.
[2] J.-M. Tarascon, M. Armand, *Nature* **2001**, *414*, 359.
[3] X. M. Li, L. F. Jiang, H. B. Zeng, *NPG Asia Mater.* **2015**, *7*, e165.
[4] S. J. Guo, S. J. Dong, *Chem. Soc. Rev.* **2011**, *40*, 2644.
[5] B. Wang, X. Li, X. Zhang, B. Luo, Y. Zhang, L. Zhi, *Adv. Mater.* **2013**, *25*, 3560.
[6] J. Chang, X. Huang, G. Zhou, S. Cui, P. B. Hallac, J. Jiang, P. T. Hurley, J. Chen, *Adv. Mater.* **2013**, *26*, 758.
[7] D. Chen, X. Mei, G. Ji, M. Lu, J. Xie, J. Lu, J. Y. Lee, *Angew. Chem. Int. Ed.* **2012**, *51*, 2409.
[8] S. Murugesan, J. T. Harris, B. A. Korgel, K. J. Stevenson, *Chem. Mater.* **2012**, *24*, 1306.
[9] N. Nitta, G. Yushin, *Part. Part. Syst. Charact.* **2014**, *31*, 317.
[10] Z. Zeng, W.-I. Liang, H.-G. Liao, H. L. Xin, Y.-H. Chu, H. Zheng, *Nano Lett.* **2014**, *14*, 1745.
[11] L. Xue, G. Xu, Y. Li, S. Li, K. Fu, Q. Shi, X. Zhang, *Appl. Mater. Interfaces* **2013**, *5*, 21.
[12] W. Wang, P. N. Kumta, *ACS Nano* **2010**, *4*, 2233.
[13] X. Zhou, Y.-X. Yin, L.-J. Wan, Y.-G. Guo, *Adv. Energy Mater.* **2012**, *2*, 1086.
[14] X. Zhao, C. M. Hayner, M. C. Kung, H. H. Kung, *Adv. Energy Mater.* **2011**, *1*, 1079.
[15] K. Evanoff, A. Magasinski, J. Yang, G. Yushin, *Adv. Energy Mater.* **2011**, *1*, 495.
[16] J. Ji, H. Ji, L. L. Zhang, X. Zhao, X. Bai, X. Fan, F. Zhang, R. S. Ruoff, *Adv. Mater.* **2013**, *25*, 4673.
[17] A. Gohier, B. Laïk, K.-H. Kim, J.-L. Maurice, J.-P. Pereira-Ramos, C. S. Cojocaru, P. T. Van, *Adv. Mater.* **2012**, *24*, 2592.
[18] H. Kim, M. Seo, M.-H. Park, J. Cho, *Angew. Chem. Int. Ed.* **2010**, *49*, 2146.
[19] H. Kim, B. Han, J. Choo, J. Cho, *Angew. Chem. Int. Ed.* **2008**, *47*, 10151.
[20] Y. Zhao, X. Liu, H. Li, T. Zhai, H. Zhou, *Chem. Commun.* **2012**, *48*, 5079.
[21] P. Gao, Y. Nuli, Y.-S. He, J. Wang, A. I. Minett, J. Yang, J. Chen, *Chem. Commun.* **2010**, *46*, 9149.
[22] X. Xin, X. Zhou, F. Wang, X. Yao, X. Xu, Y. Zhu, Z. Liu, *J. Mater. Chem.* **2012**, *22*, 7724.
[23] R. Hu, W. Sun, Y. Chen, M. Zeng, M. Zhu, *J. Mater. Chem. A* **2014**, *2*, 9118.
[24] H. Wu, G. Chan, J. W. Choi, Ryu, Y. Yao, M. T. McDowell, S. W. Lee, A. Jackson, Y. Yang, L. Hu, Y. Cui, *Nat. Nanotechnol.* **2012**, *7*, 1.
[25] M. Ko, S. Chae, S. Jeong, P. Oh, J. Cho, *ACS Nano* **2014**, *8*, 8591.
[26] X. Li, P. Meduri, X. Chen, W. Qi, M. H. Engelhard, W. Xu, F. Ding, J. Xiao, W. Wang, C. Wang, J.-G. Zhang, J. Liu, *J. Mater. Chem.* **2012**, *22*, 11014.
[27] H. Wu, G. Zheng, N. Liu, T. J. Carney, Y. Yang, Y. Cui, *Nano Lett.* **2012**, *12*, 904.
[28] X. Zhou, Y.-X. Yin, L.-J. Wan, Y.-G. Guo, *Chem. Commun.* **2012**, *48*, 2198.
[29] C. F. Sun, H. L. Zhu, M. okada, K. Gaskell, Y. Inoue, L. J. Hu, Y. H. Wang, *Nano Lett.* **2015**, *15*, 703.
[30] B. Hertzberg, A. Alexeev, G. Yushin, *J. Am. Chem. Soc.* **2010**, *132*, 8548.
[31] R. Yi, J. Zai, F. Dai, M. L. Gordin, D. Wang, *Nano Energy* **2014**, *6*, 211.
[32] Z.-S. Wu, W. Ren, L. Wen, L. Gao, J. Zhao, Z. Chen, G. Zhou, F. Li, H.-M. Cheng, *ACS Nano* **2010**, *4*, 3187.
[33] M.-H. Park, M. G. Kim, J. Joo, K. Kim, J. Kim, S. Ahn, Y. Cui, J. Cho, *Nano Lett.* **2009**, *9*, 3844.
[34] K. Evanoff, J. Benson, M. Schauer, I. Kovalenko, *ACS Nano* **2012**, *6*, 9837.
[35] L. Yin, Z. Zhang, Z. Li, F. Hao, Q. Li, C. Wang, R. Fan, Y. Qi, *Adv. Funct. Mater.* **2014**, *24*, 4176.